

PAPER

## WSe<sub>2</sub>/graphene heterojunction synaptic phototransistor with both electrically and optically tunable plasticity

To cite this article: Yilin Sun *et al* 2021 *2D Mater.* **8** 035034





View the [article online](#) for updates and enhancements.

### You may also like

- [Emerging memory technologies for neuromorphic computing](#)  
Chul-Heung Kim, Suhwan Lim, Sung Yun Woo et al.
- [High-performance synaptic transistors for neuromorphic computing](#)  
Hai Zhong, , Qin-Chao Sun et al.
- [Synaptic electronics: materials, devices and applications](#)  
Duygu Kuzum, Shimeng Yu and H-S Philip Wong



## PAPER

WSe<sub>2</sub>/graphene heterojunction synaptic phototransistor with both electrically and optically tunable plasticityRECEIVED  
18 February 2021REVISED  
4 April 2021ACCEPTED FOR PUBLICATION  
21 April 2021PUBLISHED  
13 May 2021Yilin Sun<sup>1,3</sup> , Yuxuan Lin<sup>2,3</sup> , Ahmad Zubair<sup>2</sup> , Dan Xie<sup>1,\*</sup>  and Tomás Palacios<sup>2,\*</sup><sup>1</sup> Institute of Microelectronics, Beijing National Research Center for Information Science and Technology (BNRist), Tsinghua University, Beijing 100084, People's Republic of China<sup>2</sup> Department of Electrical Engineering and Computer Science, Massachusetts Institute of Technology, Cambridge, MA 02139, United States of America<sup>3</sup> These authors contributed equally to this work.

\* Authors to whom any correspondence should be addressed.

E-mail: [xiedan@tsinghua.edu.cn](mailto:xiedan@tsinghua.edu.cn) and [tpalacios@mit.edu](mailto:tpalacios@mit.edu)**Keywords:** WSe<sub>2</sub>, graphene, synaptic phototransistor, plasticity modulationSupplementary material for this article is available [online](#)**Abstract**

The imitation of synaptic plasticity in artificial neuromorphic devices has been widely realized based on memristors, transistors and ion devices. This development of artificial synaptic devices is expected to open up a new era for neuromorphic computing. However, the complicated functions in biological synapse are dependent on the dynamic neural activities with modulated plasticity, which is still very difficult to emulate at the device level. Here, an artificial synaptic transistor based on WSe<sub>2</sub>/graphene van der Waals heterojunction is demonstrated with both electrically and optically modulated synaptic plasticity. By changing the polarity of applied  $V_{gs}$  and  $V_{ds}$  as well as superimposed gate voltage spikes, both excitatory and inhibitory synaptic plasticity can be realized in a single device. Moreover, due to the asymmetric optical response of WSe<sub>2</sub>/graphene heterojunction, optical modulation on hysteretic behaviors is achieved and also contributes to the inversion of synaptic plasticity. Hence, this work demonstrates a coordinated regulation on synaptic plasticity under electrical and optical stimuli and provides a multi-dimensional modulation strategy to understand the underlying mechanisms of complicated neuromorphic computing and further develop multifunctional neuromorphic optoelectronics.

**1. Introduction**

Synaptic electronics use nanoscale neuromorphic devices to emulate the memory or learning behaviors in humans [1–3]. In biological systems, synaptic functions are realized based on plasticity, i.e. the adjustable response of connection strength, known as synaptic weight, of two adjacent neurons under pre-synaptic stimuli [4, 5]. Two well-known types of synaptic plasticity are short-term plasticity (STP) and long-term plasticity (LTP), where STP refers to a temporal change of synaptic weight but LTP indicates a permanent change of synaptic weight [6]. The most distinctive feature for this property is the time-varying strengthened or weakened synaptic weight induced by different neural activity, resulting in synaptic potentiation and depression, respectively [7, 8]. Inspired by the superiority of biological synapse in

neuromorphic computing and information storage, great efforts have been devoted to developing artificial synaptic devices such as two-terminal memristors [9–11] and field effect transistors [12–14] to emulate the synaptic plasticity. In such devices, electric spikes are often applied as pre-synaptic stimuli on one terminal of devices and the conductances or currents triggered by these electric stimuli are recorded as post-synaptic current (PSC), which describes the synaptic weight change of biological synapse under the pre-synaptic stimuli.

However, the dynamics of artificial synaptic devices have not been fully achieved, which is essential for the complicated behaviors of living creatures [15]. A typical biological synapse is expected to have the ability to express the synaptic plasticity in a tunable way [16]. A wide variety of synaptic devices in the literature implement static plasticity by using

electric stimuli to trigger the continuous and non-volatile change of conductance [17–19], while the realization of plasticity modulation is still not well explored. Recently, several strategies have been proposed to modulate synaptic plasticity, which can be classified as two directions. First, both STP and LTP may be directly tuned by changing the chemical composition of functional materials [17, 18]. In this way, the electrical or optical properties of the materials can be modulated by changing the ion concentration, resulting in a tunable plasticity from device to device. Because the chemical composition is always pre-defined during the material synthesis, the difference in plasticity could only be observed in different devices rather than in a single device, which is inconsistent with the properties of biological synapse in which the plasticity of a given synapse can be tuned *in-situ*. Second, in some devices, a bottom gate is often used to modulate the overall conductance of the device, which offers an opportunity for synaptic transistors to change its weight. By this way, an electrically tunable method can be used to achieve tunable plasticity by changing the polarity of bottom gate voltages to achieve synaptic dynamics, leading to the conversion between inhibitory synaptic plasticity (synaptic depression) and excitatory synaptic plasticity (synaptic potentiation) in a single device [19]. Besides, a top-gate graphene–ferroelectric transistor has been proposed to realize both potentiative and depressive synapse based on ambipolar transport characteristics of graphene and ferroelectric polarization tuned by gate voltage [20]. Plasticity modulation controlled by independent gates is successful in mimicking the multilevel dynamics of biological synapses. Although the electrical modulation of plasticity is well demonstrated, double-gated structures where the pre-synaptic stimuli is applied on the top gate and the control signal is applied on the bottom gate significantly increases the complexity of both the device structure and the operation.

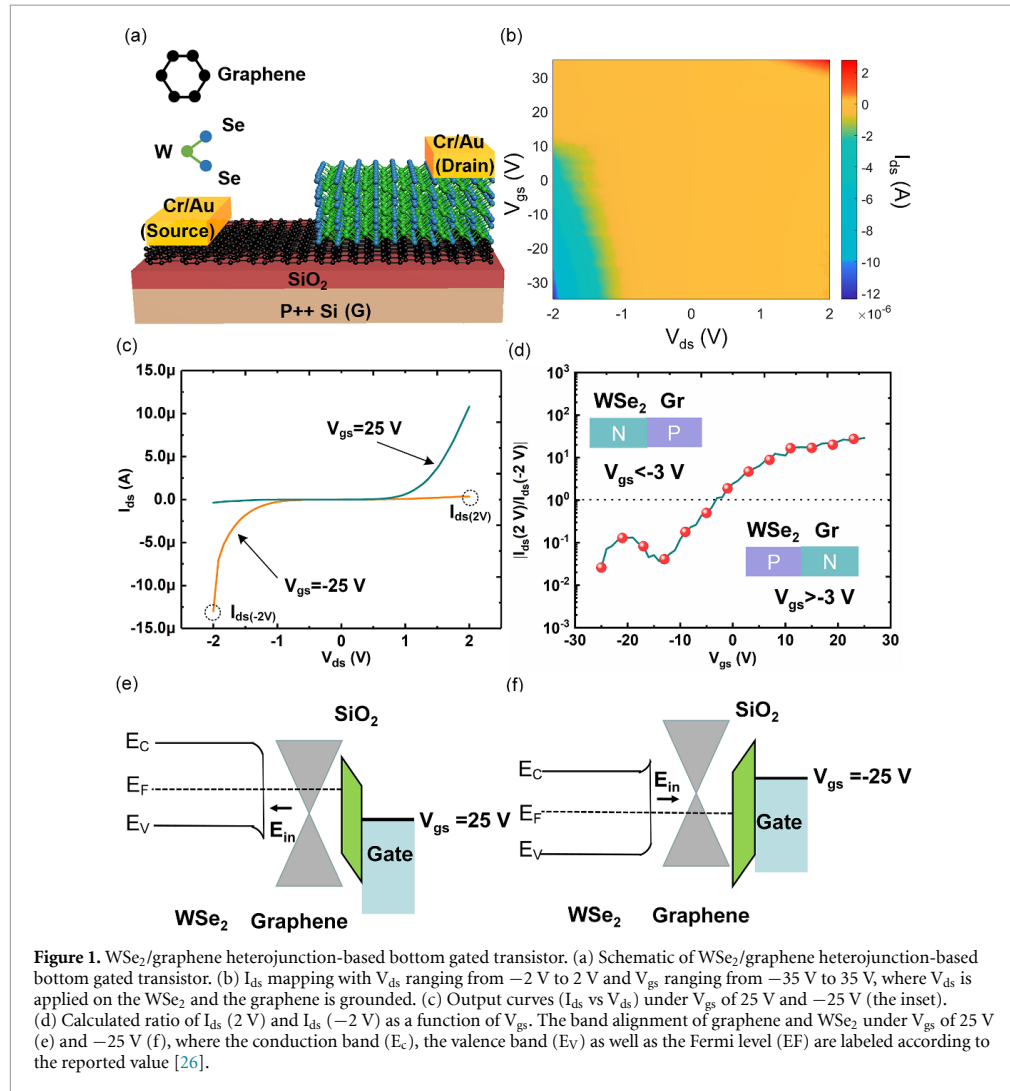
In parallel to the work on electrical modulations, optically stimulated synaptic devices have also recently been demonstrated with the ability to emulate the synaptic plasticity, where the conductance of functional layer can respond to optical stimuli in a synapse-like way [21–25]. The optically stimulated synapses open up an alternative way to integrate synaptic plasticity and optical information sensing into one single device. However, the optical modulation on the synaptic plasticity has not been well studied.

In this paper, we propose a novel strategy for synergistic electrical and optical modulation of the synaptic plasticity. A synaptic phototransistor based on WSe<sub>2</sub>/graphene heterojunction is demonstrated with both electrically and optically tunable synaptic plasticity. By changing the polarity of applied electrical spikes on the bottom gate, a conversion between inhibitory synapse and excitatory synapse is achieved. Besides, optical modulation is also

implemented in the synaptic phototransistor to realize the inhibitory/excitatory plasticity conversion. The presented WSe<sub>2</sub>/graphene heterojunction synaptic phototransistor with electrically and optically tunable synaptic plasticity offers a unique opportunity to understand the physical principles of neuromorphic devices with complex functions and to explore novel optoelectronic devices.

## 2. Results and discussion

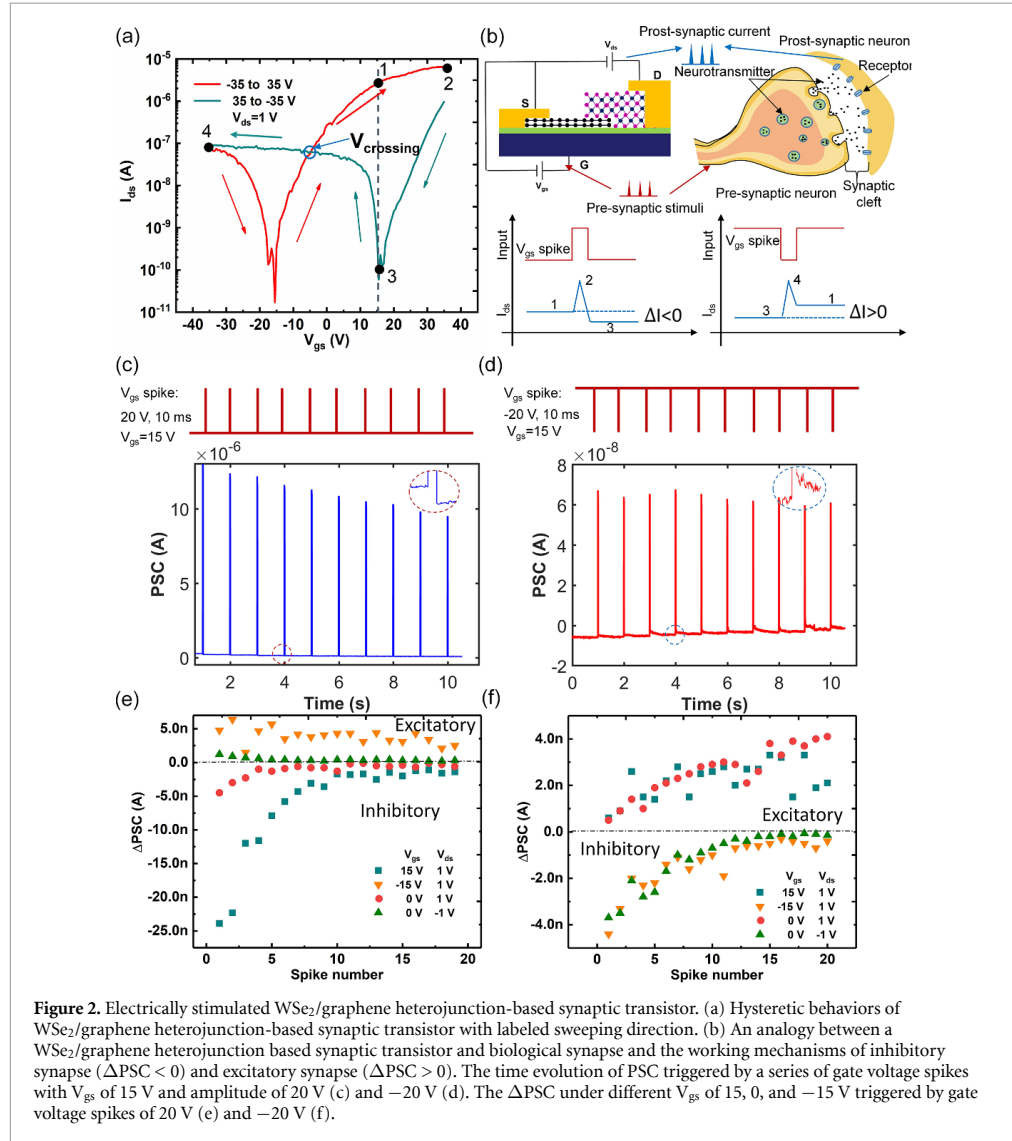
The schematic of the bottom-gated synaptic phototransistor based on a vertical WSe<sub>2</sub>/graphene heterojunction is shown in figure 1(a) (see the experimental section). The optical micrograph of the as-fabricated device is shown in figure S1(a) (available online at [stacks.iop.org/2DM/8/035034/mmedia](https://stacks.iop.org/2DM/8/035034/mmedia)). The overlapping area between the graphene and the WSe<sub>2</sub> flake forms the vertical heterojunction. The thickness of both graphene and WSe<sub>2</sub> is 1.2 nm and 74.8 nm, respectively, according to atomic force microscopic images (see figure S1(b), supporting information). Raman spectra of graphene and WSe<sub>2</sub> further confirm their multi-layered structure (see figure S2, supporting information). To characterize the electrical performance, a channel current ( $I_{ds}$ ) map as a function of  $V_{ds}$  and  $V_{gs}$  is measured and shown in figure 1(b), indicating rectifying behaviors tuned by the bottom gate. Typical rectifying behaviors with different polarities under the  $V_{gs}$  of 25 V and –25 V can be found in figure 1(c), indicating the existence of a reconfigurable p–n junction. The gate modulation effect can be further manifested by the ratio of  $I_{ds}$  under  $V_{gs}$  of 2 V and –2 V as shown in figure 1(d). It can be seen that the ratio increases from  $10^{-2}$  to  $10^2$  with increased  $V_{gs}$  and achieves a value of 1 at  $V_{gs}$  of –3 V, which suggests an ambipolar transport behavior of the WSe<sub>2</sub>/graphene heterojunction. When  $V_{gs} < -3$  V, the WSe<sub>2</sub>/graphene heterojunction is switched on under a negative  $V_{ds}$ , which can be regarded as a N(WSe<sub>2</sub>)–P(graphene) junction. When  $V_{gs} > -3$  V, the junction is switched on under a positive  $V_{ds}$ , indicating a P(WSe<sub>2</sub>)–N(graphene) junction. Such gate-tunable rectifying behaviors can be well understood by the band alignment between graphene and WSe<sub>2</sub> under different  $V_{gs}$  as shown in figures 1(e) and (f). The WSe<sub>2</sub>/graphene hybrid channel can be divided as three parts: standalone WSe<sub>2</sub>, WSe<sub>2</sub>/graphene heterojunction and standalone graphene, where the standalone WSe<sub>2</sub> and graphene parts work as two  $V_{gs}$ -tunable resistors and would not change the direction of rectification [26]. Therefore, the rectifying characteristics are dominated by the WSe<sub>2</sub>/graphene heterojunction, where the Fermi level of the underlying graphene can be modulated more efficiently by bottom-gate voltage  $V_{gs}$  compared with the upper WSe<sub>2</sub> because of the lower density of states when the graphene is intrinsic, and the electrostatic



screening when graphene is doped [27]. A positive  $V_{gs}$  (figure 1(e)) induces an n-type doping in graphene while WSe<sub>2</sub> stays intrinsic, resulting in a built-in electric field pointing from the graphene side toward the WS<sub>2</sub> side, which corresponds to a P(WSe<sub>2</sub>)–N(graphene) junction. On the other hand, when  $V_{gs}$  is negative (figure 1(f)), graphene becomes p-doped while WSe<sub>2</sub> remains intrinsic, which then reverses the built-in electric field and the polarity of the junction (a N–P junction).

The ambipolar transfer curves of WSe<sub>2</sub>/graphene heterojunction based bottom-gated transistor are shown in figure 2(a). An obvious hysteretic behavior with respect to  $V_{gs}$  can be observed with a large memory window of about 30 V (defined as the shift in  $V_{gs}$  for a given current level in the forward and reversed sweeping direction). There is a crossing point for the forward and reversed curves, which is denoted as  $V_{crossing}$ . The hysteretic behaviors have

been considered as a basic requirement for memory device [28] and the origin of hysteretic behaviors of 2D semiconductor-based FET devices is widely attributed to the dynamic response of the trapped charges at the interface of the heterojunction under an external electric field [29–31]. To evaluate the hysteretic characteristics of as-fabricated WSe<sub>2</sub>/graphene heterojunction, the dynamics of observed hysteretic behaviors have been investigated. It is also observed that the hysteretic window becomes narrower with a faster gate voltage ramping rate or a smaller sweeping range, which is consistent with the charge trapping/de-trapping process (see figures S3(a) and (b), supporting information) [32–34]. Recently, synaptic behaviors based on pronounced hysteresis that mimic the synaptic plasticity have also been well investigated [35–37]. Based on it, an analogy between a WSe<sub>2</sub>/graphene heterojunction synaptic transistor and a biological synapse is shown in figure 2(b),



where the gate voltage spikes are regarded as pre-synaptic stimuli and the current flowing through WSe<sub>2</sub>/graphene heterojunction is regarded as the PSC. Once the voltage spike is applied onto the bottom gate electrodes, the induced carriers generate a sudden change of  $I_{ds}$ . This operation may be seen as a fast gate voltage sweeping, which will cause the change of  $I_{ds}$  at the end of the voltage spike as described by the corresponding point of hysteresis curve in figure 2(a). For example, when a positive gate voltage spike with the amplitude of 20 V is applied onto the bottom gate, the  $V_{gs}$  rapidly increasing from 15 V to 35 V,  $I_{ds}$  will increase from point 1 to point 2 at the rising edge of the voltage spike and recover to point 3 at the falling edge. It can be expected that the value of  $I_{ds}$  at point 3 is smaller than that at point 1. The value of  $I_{ds}$  can be used to emulate the synaptic

weight and its decrease reflects the change of PSC ( $\Delta PSC$ ), which is known as synaptic plasticity. When a negative gate voltage spike with the amplitude of  $-20$  V is applied onto  $V_{gs}$  of 15 V,  $I_{ds}$  changes from point 3 to point 4 and recovers to point 1, indicating an increase of  $I_{ds}$  and positive  $\Delta PSC$ . The polarity of  $\Delta PSC$  can be determined by the direction of applied gate voltage spike and its amplitude is manifested by the relative position of two different  $I_{ds}$  values under the same  $V_{gs}$  in hysteresis curve. In other words, the polarity of  $\Delta PSC$  depends on the relative position between  $V_{gs}$  (the baseline of voltage spike) and  $V_{crossing}$ . Figures 2(c) and (d) exhibit the dynamic response of  $I_{ds}$  under a series of gate voltage spikes of 20 V with different polarity applied on the  $V_{gs}$  of 15 V (to the right of the  $V_{crossing}$ ), where opposite  $\Delta PSC$ s are obtained in consistency with the

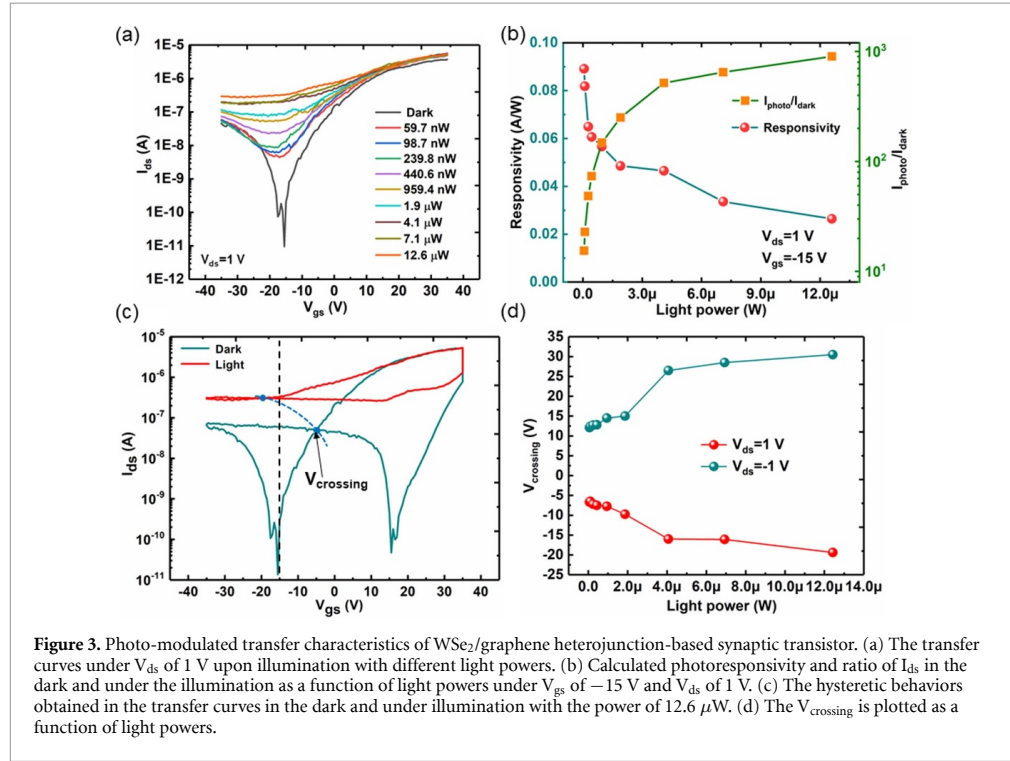


**Figure 3.** Photo-modulated transfer characteristics of WSe<sub>2</sub>/graphene heterojunction-based synaptic transistor. (a) The transfer curves under  $V_{ds}$  of 1 V upon illumination with different light powers. (b) Calculated photoresponsivity and ratio of  $I_{ds}$  in the dark and under the illumination as a function of light powers under  $V_{gs}$  of  $-15$  V and  $V_{ds}$  of 1 V. (c) The hysteretic behaviors obtained in the transfer curves in the dark and under illumination with the power of  $12.6 \mu\text{W}$ . (d) The  $V_{\text{crossing}}$  is plotted as a function of light powers.

hysteretic behaviors. In this way, the synaptic plasticity, which determines the response of biological synapse to neural activities from previous neurons, can be achieved. Moreover, positive  $\Delta\text{PSC}$  always indicates an enhanced synaptic weight and excitatory synaptic plasticity while negative  $\Delta\text{PSC}$  indicates a decreased synaptic weight and inhibitory synaptic plasticity. Therefore, both excitatory and inhibitory synaptic plasticity can be realized in a single device by changing the polarity of applied gate voltage spikes.

It is observed that the synaptic plasticity can be modulated by a variety of electrical signals. We have shown the modulation by changing the polarity of gate voltage spikes for the certain  $V_{gs}$  and  $V_{ds}$ . In the following, we present that such excitatory–inhibitory plasticity conversions can also be achieved through  $V_{gs}$  and  $V_{ds}$  control. The time evolution of PSC triggered by a series of gate voltage spikes under different  $V_{gs}$  and  $V_{ds}$  are shown in figures S4 and S5, from which  $\Delta\text{PSC}$  as a function of the gate voltage spike number under different  $V_{gs}$  and  $V_{ds}$  as well as the polarity of the gate voltage spikes are extracted and summarized in figures 2(e) and (f). The  $V_{gs}$  dependence of synaptic plasticity can be understood by the relative position between  $V_{gs}$  and  $V_{\text{crossing}}$ , and the resulting hysteresis loop for a given gate voltage spike, similar to the spike polarity dependence as discussed above. It is noted that the conversion of plasticity with  $V_{ds}$  changing from 1 V to  $-1$  V under the  $V_{gs}$  of 0 V can be attributed to the shift of  $V_{\text{crossing}}$  from a negative value to a positive one induced by the

voltage dependent rectification characteristics of the WSe<sub>2</sub>/graphene heterojunction discussed above (see figure S6, supporting information). These voltage-dependent operations for plasticity modulation has been summarized (see table S1, supporting information). Our results demonstrate a feasible and simple method to achieve multimodal plasticity modulations under different configurations of electrical signals, which may contribute to the emulation of complex neural activities in real biological synapses.

We further explore the photoresponse of such an unique electrical multimodal synaptic transistor and discuss the possibility of the optical modulation on the synaptic plasticity. Figure 3(a) shows a set of transfer characteristics of the bottom-gated WSe<sub>2</sub>/graphene heterojunction under illumination with different powers. A significant enhancement in  $I_{ds}$  is obtained only at negative  $V_{gs}$ , indicating an asymmetric optical response similar to that of photo-diodes based on P–N junction [38]. From figure 1(f), when  $V_{gs}$  at a negative value, a p–n like junction exist between graphene and WSe<sub>2</sub> due to the gate voltage induced holes accumulation in graphene layer, forming a built-in field from WSe<sub>2</sub> to graphene. Such built-in field can be strengthened with a positive  $V_{ds}$  applied on WSe<sub>2</sub>. The remarkable photocurrent generated at the region of  $V_{gs} < 0$  in figure 3(a) can be attributed to the optimized separation of photo-generated carriers accelerated by the increased built-in field. Similar asymmetric optical response can be also observed at  $V_{ds}$  of  $-1$  V, where the



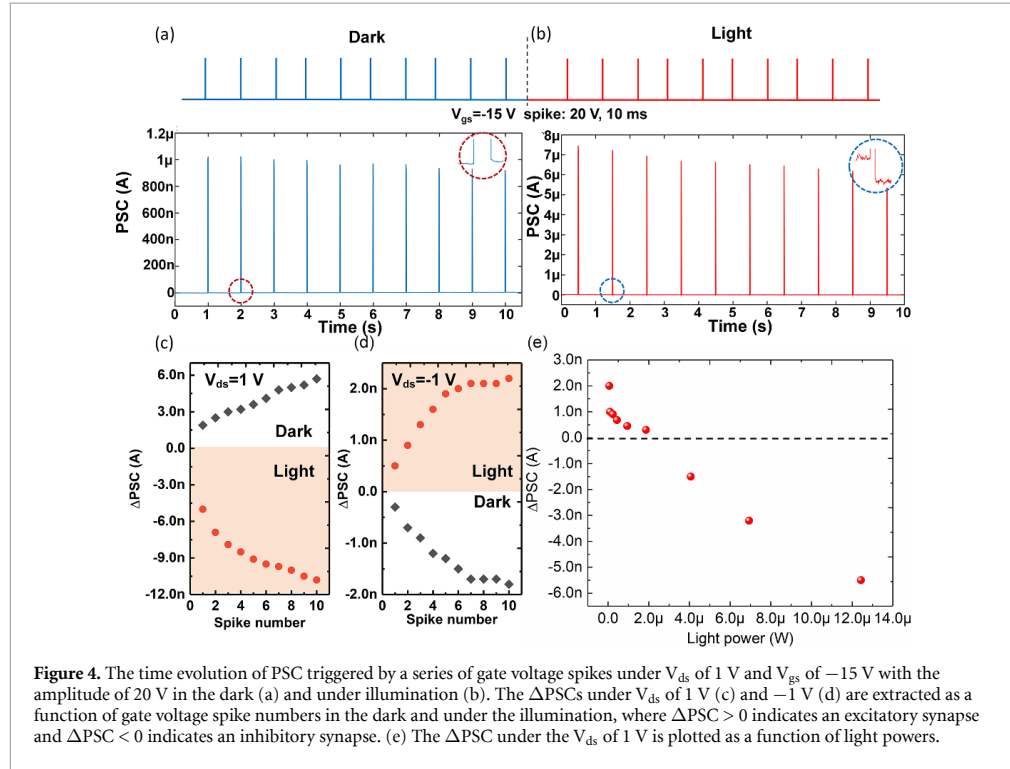


**Figure 4.** The time evolution of PSC triggered by a series of gate voltage spikes under  $V_{ds}$  of 1 V and  $V_{gs}$  of  $-15$  V with the amplitude of 20 V in the dark (a) and under illumination (b). The  $\Delta$ PSCs under  $V_{ds}$  of 1 V (c) and  $-1$  V (d) are extracted as a function of gate voltage spike numbers in the dark and under the illumination, where  $\Delta$ PSC  $> 0$  indicates an excitatory synapse and  $\Delta$ PSC  $< 0$  indicates an inhibitory synapse. (e) The  $\Delta$ PSC under the  $V_{ds}$  of 1 V is plotted as a function of light powers.

enhanced photocurrent occurs for positive  $V_{gs}$  (see figure S7, supporting information). The photocurrent responsivity and the ratio of  $I_{ds}$  in the dark and under the illumination are calculated as a function of the incident light power as shown in figure 3(b). The maximum responsivity is about  $0.9 \text{ A W}^{-1}$  and decreases with light power, which is consistent with reported photodetectors with similar structure [25]. The ratio of  $I_{ds}$  in the dark and under the illumination increases with light power and reaches a saturation value of  $10^3$ .

Considering the asymmetric photocurrent response of the WSe<sub>2</sub>/graphene heterojunction, we investigate the optical modulation on the hysteretic behaviors. Upon illumination, the hysteresis loop exhibits a shape change as shown in figure 3(c). An important feature is the shift of  $V_{crossing}$  under illumination, which can be also observed for  $V_{ds}$  of  $-1$  V (see figure S7, supporting information). We have demonstrated that the polarity of synaptic plasticity can be modulated by applied gate voltage spikes and the baseline of  $V_{gs}$  according to their relative positions with respect to  $V_{crossing}$  and the corresponding hysteresis loops. It can be inferred that the crossing point shift of the hysteresis loop under the illumination may also induce the inversion of synaptic plasticity. For example, the relative position of  $I_{ds}$  in the dark at  $V_{gs}$  of  $-15$  V indicates a positive  $\Delta$ PSC when a positive gate voltage spike applied. However,  $\Delta$ PSC may become negative under

illumination under the same electrical bias conditions due to the shift of the  $V_{crossing}$ , which is caused by the asymmetric optical response of WSe<sub>2</sub>/graphene heterojunction. Moreover, the shift of  $V_{crossing}$  may be directly affected by the light power as shown in figure 3(d), where a positive shift of the  $V_{crossing}$  can be obtained under the  $V_{ds}$  of  $-1$  V and a negative shift of the  $V_{crossing}$  is obtained under the  $V_{ds}$  of 1 V.

In this way, optical stimuli can be used as another physical domain of modulation to realize the dynamics of synaptic plasticity. We applied a series of positive gate voltage spikes of  $V_{gs} = -15$  V to trigger the PSC in darkness (figure 4(a)) and under illumination (figure 4(b)). A polarity change of  $\Delta$ PSC from positive to negative is achieved upon illumination, indicating a conversion from excitatory to inhibitory plasticity. The opposite conversion can be achieved under the  $V_{ds}$  of  $-1$  V, where a series of positive gate voltage spikes is applied on the  $V_{gs}$  of 15 V and a conversion from inhibitory to excitatory plasticity is realized upon illumination (see the figure S8, supporting information). In figures 4(c) and (d),  $\Delta$ PSC is plotted as a function of gate voltage spike numbers in dark and under illumination under different voltage bias, where  $\Delta$ PSC stays positive value when in dark and is reversed to negative values under illumination when  $V_{ds}$  is 1 V while the opposite change is achieved under the  $V_{ds}$  of  $-1$  V. This optical modulated synaptic plasticity can be explained by the photo-induced

shift of  $V_{\text{crossing}}$ . It is noted that the shift of  $V_{\text{crossing}}$  is dependent on the incident light power. Therefore, the  $\Delta\text{PSC}$  is also measured as a function of light power as shown in figure 4(e), where  $\Delta\text{PSC}$  is still a positive value for power levels below  $2 \mu\text{W}$  because  $V_{\text{gs}} (-15 \text{ V})$  is still to the left of  $V_{\text{crossing}}$  as shown in figure 3(d). With the increase of the incident light power,  $V_{\text{crossing}}$  continuously decreases and finally becomes smaller than  $V_{\text{gs}} (-15 \text{ V})$ , namely  $V_{\text{gs}}$  becomes larger than  $V_{\text{crossing}}$  and its position in hysteric loop is shifted to the right of  $V_{\text{crossing}}$ , resulting in the polarity change of  $\Delta\text{PSC}$ . In this way, the optical stimuli can be another variable to reverse synaptic plasticity.

It is noted that the optical modulation on the synaptic plasticity is conditional. When  $V_{\text{ds}}$  is 1 V and  $V_{\text{gs}}$  is 0 V or 15 V, which is larger than  $V_{\text{crossing}}$  and their position in hysteric loop is always to the right of  $V_{\text{crossing}}$  both in dark and under illumination, the polarity of  $\Delta\text{PSC}$  will not change under the optical modulation. The similar result can be found when  $V_{\text{ds}}$  is 1 V and  $V_{\text{gs}}$  is 0 V or  $-15 \text{ V}$ . This means that there is a non-trivial cross correlation between the electrical and the optical modulation and the above results also highlight the electrical and optical coordinated modulation on synaptic plasticity, providing a feasible strategy to build multifunctional neuromorphic devices implanted with complicated functions.

### 3. Conclusion

In summary, the electrically and optically coordinated modulation on the synaptic plasticity is achieved in a gate reconfigurable  $\text{WSe}_2/\text{graphene}$  heterojunction phototransistor, based on its unique carrier transport and optoelectronic characteristics with pronounced hysteric behaviors. Both excitatory and inhibitory synaptic plasticity are imitated in a single device and a complex mapping from electrical control (through gate voltage, drain voltage, and the polarity of the gate voltage spikes) to plasticity is realized. The asymmetric photo response of  $\text{WSe}_2/\text{graphene}$  heterojunction results in the nontrivial shape change of the hysteresis loop, which can reverse the plasticity. In this way, plasticity modulation can be realized both electrically and optically. Our device introduces an optimized structure for artificial neuromorphic optoelectronics and offers a novel strategy for the design of artificial synaptic devices with tunable plasticity for complicated neuromorphic computing.

### 4. Methods

#### 4.1. Device fabrication of $\text{WSe}_2/\text{graphene}$ heterojunction-based bottom gated transistor

Graphene flakes and  $\text{WSe}_2$  flakes were obtained by a mechanical exfoliation onto the  $\text{SiO}_2/\text{Si}$  substrate and the  $\text{WSe}_2$  flake picked using optical

microscopy was then transferred to a designed area on the top of previously prepared graphene flake, where a poly(bisphenol A carbonate) (PC)/polydimethylsiloxane stack on a glass slide mounted on a custom-made micro-positioning stage was used to pick up the  $\text{WSe}_2$  flake from  $\text{SiO}_2/\text{Si}$  substrate and release it on the graphene flake by controlling the temperature of substrate. Finally, the substrate was cleaned in the chloroform to remove residual PC and graphene flake and  $\text{WSe}_2$  flake was combined with each other by van der Waals force between them. Electron beam lithography was used to pattern the active area and drain-source electrodes were deposited by electron beam evaporation with Ti/Au.

#### 4.2. Characterizations of $\text{WSe}_2/\text{graphene}$ heterojunction-based bottom gated transistor

The device was wire-bonded onto a chip carrier with electrical connections and measured in a Janis cryostat with a vacuum level of  $10^{-5}$  Torr. The electrical characterizations were performed with sourcemeters (Agilent B2902a, B1500A, 2614B), current preamplifiers (Ithaco DL1211), and data acquisition cards (National Instruments PXI module). The monochromic light of 628 nm is generated from a broadband supercontinuum fiber laser (Fianium) and a monochromator to generate the monochromic laser beam with the desired wavelength and coupled to a microscope and a  $60\times$  objective lens with correction ring (Olympus,  $\text{NA} = 0.7$ ), which helps investigate the photo-modulated transport characteristics of our device and a light-emitting illumination device (CEL-LEDS35 CEL-LEDS35) is applied to generate monochromic light of 660 nm to study the optically modulated synaptic plasticity.

#### Data availability statement

The data that support the findings of this study are available upon reasonable request from the authors.

#### Acknowledgments

Y S and D X grateful for the financial support from the National Natural Science Foundation of China (No. 52072204), the National Key R&D Program of China (2016YFA0200200) and National Postdoctoral Program for Innovative Talents of China (BX20200049). Y L and T P acknowledge the partial support by the US Army Research Office through the Institute for Soldier Nanotechnology at MIT, under cooperative number W911NF-18-2-0048, and the NSF-funded STC Center for Integrated Quantum Materials, NSF Grant No. DMR-1231319. We thank Dr Qiong Ma and Professor Pablo Jarillo-Herrero for assisting with the optical setup.



## Competing financial interests

The authors declare no competing financial interests

## ORCID iDs

Yilin Sun  <https://orcid.org/0000-0001-9390-4030>

Yuxuan Lin  <https://orcid.org/0000-0003-0638-2620>

Ahmad Zubair  <https://orcid.org/0000-0001-9827-3557>

Dan Xie  <https://orcid.org/0000-0001-9521-9774>

## References

- [1] van de Burgt Y, Lubberman E, Fuller E J, Keene S T, Faria G C, Agarwal S, Marinella M J, Talin A A and Salleo A 2017 *Nat. Mater.* **16** 414–8
- [2] Balakrishna Pillai P and de Souza M M 2017 *ACS Appl. Mater. Interfaces* **9** 1609–18
- [3] Park Y and Lee J S 2017 *ACS Nano* **11** 8962–9
- [4] Bi G and Poo M 1998 *J. Neurosci.* **18** 10464–72
- [5] Zhu L Q, Wan C J, Guo L Q, Shi Y and Wan Q 2014 *Nat. Commun.* **5** 3158
- [6] Hu L, Fu S, Chen Y, Cao H, Liang L, Zhang H, Gao J, Wang J and Zhuge F 2017 *Adv. Mater.* **29** 1606927
- [7] Zhong Y N, Wang T, Gao X, Xu J L and Wang S D 2018 *Adv. Funct. Mater.* **28** 1800854
- [8] Kim K, Chen C L, Truong Q, Shen A M and Chen Y 2013 *Adv. Mater.* **25** 1693–8
- [9] Zeng F, Guo Y, Hu W, Tan Y, Zhang X, Feng J and Tang X 2020 *ACS Appl. Mater. Interfaces* **12** 23094–101
- [10] Dang B, Wu Q, Song F, Sun J, Yang M, Ma X, Wang H and Hao Y 2018 *Nanoscale* **10** 20089–95
- [11] Zhu X, Li D, Liang X and Lu W D 2019 *Nat. Mater.* **18** 141–8
- [12] Yang C S, Shang D S, Liu N, Shi G, Shen X, Yu R C, Li Y Q and Sun Y 2017 *Adv. Mater.* **29** 1700906
- [13] Yang C S, Shang D S, Liu N, Fuller E J, Agrawal S, Talin A A, Li Y, Shen B and Sun Y 2018 *Adv. Funct. Mater.* **28** 1804170
- [14] Paul T, Ahmed T, Tiwari K K, Thakur C S and Ghosh A 2019 *2D Mater.* **6** 045008
- [15] Meyer A C et al 2009 *Nat. Neurosci.* **12** 444–53
- [16] Abraham W C 2008 *Nat. Rev. Neurosci.* **9** 387
- [17] Lv D, Yang Q, Chen Q, Chen J, Lai D, Chen H and Guo T 2019 *Nanotechnology* **31** 065201
- [18] Sun Y, Qian L, Xie D, Lin Y, Sun M, Li W, Ding L, Ren T and Palacios T 2019 *Adv. Funct. Mater.* **29** 1902538
- [19] Tian H, Mi W, Wang X F, Zhao H, Xie Q Y, Li C, Li Y, Yang Y and Ren T L 2015 *Nano Lett.* **15** 8013–9
- [20] Chen Y, Zhou Y, Zhuge F, Tian B, Yan M, Li Y, He Y and Miao X S 2019 *npj 2D Mater. Appl.* **3** 31
- [21] Qin S, Wang F, Liu Y, Wan Q, Wang X, Xu Y, Shi Y, Wang X and Zhang R 2017 *2D Mater.* **4** 035022
- [22] Ahmed T, Kuriakose S, Mayes E L, Ramanathan R, Bansal V, Bhaskaran M, Sriram S and Walia S 2017 *Small* **15** 1900966
- [23] Zhou F et al 2019 *Nat. Nanotechnol.* **14** 776–82
- [24] Wang Y, Lv Z, Chen J, Wang Z, Zhou Y, Zhou L, Chen X and Han S T 2018 *Adv. Mater.* **30** 1802883
- [25] Li H, Jiang X, Ye W, Zhang H, Zhou L, Zhang F, She D, Zhou Y and Han S T 2019 *Nano Energy* **65** 104000
- [26] Gao A, Liu E, Long M, Zhou W, Wang Y, Xia T, Hu W, Wang B and Miao F 2016 *Appl. Phys. Lett.* **108** 223501
- [27] Castro Neto A H, Guinea F, Peres N M R, Novoselov K S and Geim A K 2009 *Rev. Mod. Phys.* **81** 109
- [28] Lee Y, Um D S, Lim S, Lee H, Kim M P, Yang T-Z, Chueh Y-L, Kim H and Ko H 2019 *ACS Appl. Mater. Interfaces* **11** 23382–91
- [29] Huo N, Yang J, Huang L, Wei Z, Li S S, Wei S H and Li J 2015 *Small* **11** 5430–8
- [30] Iqbal M Z, Siddique S and Abideen Z 2017 *Carbon* **123** 168–73
- [31] Guo J, Wang L, Yu Y, Wang B, Huang Y and Duan X 2019 *Adv. Mater.* **31** 1902962
- [32] Feng W, Zheng W, Chen X, Liu G and Hu P A 2015 *ACS Appl. Mater. Interfaces* **7** 26691–5
- [33] Kumar A S, Wang M, Li Y, Fujita R and Gao X P A 2020 *ACS Appl. Mater. Interfaces* **12** 46854–61
- [34] Shu J, Wu G, Guo Y, Liu B, Wei X and Chen Q 2016 *Nanoscale* **8** 3049
- [35] Kim S, Yoon J, Kim H D and Choi S J 2015 *ACS Appl. Mater. Interfaces* **7** 25479–86
- [36] Jiang J, Guo J, Wan X, Yang Y, Xie H, Niu D, Yang J, He J, Gao Y and Wan Q 2017 *Small* **13** 1700933
- [37] Wang H et al 2018 *Adv. Mater.* **30** 1803961
- [38] Sun M et al 2018 *Nano Res.* **11** 3222